




Solar Irradiance Variability, Influenced by r Modes

Charles L. Wolff 

Solar Physics Laboratory, NASA Goddard Space Flight Center, Greenbelt, MD 20771, USA; Charles.L.Wolff@nasa.gov
Received 2018 September 14; revised 2018 October 31; accepted 2018 November 1; published 2018 December 28

Abstract

A spectrum of the four-decade solar irradiance record has a prominent cluster of power for periodicities near 1 yr. Correlating irradiance with a bandpass filter showed that periodicity values were not constant, but varied sinusoidally with each cycle lasting 14 ± 1 yr. The large modulation amplitude makes solar frequencies $\geq 1 \text{ yr}^{-1}$ hard to detect at the solar surface. After removing the modulation, a Lomb–Scargle spectrum exposed two true periodicities: 1.006 and 0.920 yr. They are interpreted as the synodic rotation periods of r modes of lowest angular degree ($\ell = 1$). The first propagates in the stable interior and the second in the convective envelope perturbed by its several flow fields. The rotational beat period of the two modes is about 10.9 yr. This is close to the average length of a solar cycle and possibly controls this average. The 1.006 yr periodicity dominates most of the filtered irradiance record but an abrupt change to about 0.8 yr occurs in mid-2010. Also found was evidence for higher-degree r modes ($\ell = 2$ to 8) and a curious sawtooth modulation with a recurrence period of 2.6 yr.

Key words: Sun: activity – Sun: interior – Sun: oscillations

1. Introduction

Solar energy flux has been well monitored from space for about 40 yr. The total solar irradiance (TSI) is defined at exactly 1 au and its combined record comes from various groups of experimenters whose work overlaps in time, permitting much cross calibration. Three families of detectors are relevant here: the HF device on NIMBUS (Hickey et al. 1980), the ACRIM versions on SMM and UARS (Willson & Hudson 1988), and Virgo on *SOHO* (Frohlich et al. 1997).

Impressive efforts to place these observations on a single intensity scale have resulted in three TSI composite series: ACRIM (Willson & Mordvinov 2003), IRMB (DeWitte et al. 2004), and PMOD (Frohlich 2006). The PMOD file is used here. It extends as far as possible into the past by utilizing the early HF data (corrected for decay in its sensitivity). It supplies daily values of TSI from 1978 November 17 to 2017 September 20. Missing days were filled in with the last available value. It is called composite_42_65_1709.dat and is posted at <ftp://pmodwrc.ch/pub/data/irradiance/composite/DataPlots>.

Total solar irradiance is seen to vary on timescales of weeks up to a decade. It plainly shows sharp dips in brightness over just a few days that can last a week or more. The 27 day rotational modulation and the 11 yr solar cycle period are prominent. A roughly 1 yr recurrence is even discernible on plots of daily TSI for a few years near 2002.

The presence or absence of 1 yr periodicities have been claimed for various solar data sets, but results often depend on the beginning and end points of the time series. This suggests, for example, an intermittent phenomenon or one with time-variable periodicity or amplitude. Lean & Brueckner (1989) found a 350 day period in 31 years of several solar activity records. Oliver et al. (1992) found the same periodicity in a detailed study of one century of daily sunspot areas and sunspot numbers. Measurements of solar radius from space show a strong periodicity near 1 yr (Bush et al. 2010), which Qu & Xie (2013) reveal as a closely spaced triplet. Much earlier, Kotov & Levitsky (1983) found a close triplet near 1 yr in a half-century of interplanetary magnetic field observations.

This paper seeks to clarify the TSI spectrum at annual-scale frequencies and higher. It is motivated by the possibility that real periodicities exist deep inside the Sun caused by globally coherent oscillations trapped below the Sun’s convective envelope (CE). Beats between their differing rotation periods would deposit thermal energy on a regular schedule, which is of special interest near the base of the CE. Much of their effect would be detected imperfectly and with some delay only after it transits the CE.

Evidence for r modes was offered by Kuhn et al. (2000), who suggest high harmonic modes cause hills on the Sun, and by Sturrock et al. (2014), who report periodicities due to low harmonics for odd ℓ in radioactive decay rates on Earth. Spectral analysis, below, indicates that r modes also modulate the Sun’s irradiance.

2. Some Properties of r Modes

If there are many global oscillations active below the CE, then there will be many internal solar recurrence periods. The low harmonic r modes will have extreme stability as most of the solar mass participates in their motion. For this reason some periodicities in Section 3 are compared to “clocks” that keep perfect time during the few decades of TSI data.

Solar r modes are primarily horizontal oscillations responding mainly to the Coriolis restoring force. Their surface velocity distribution is $\mathbf{r} \times \nabla Y$, where Y is a spherical harmonic function, $Y_{\ell,m}(\theta, \phi)$. There is no $\ell = 0$ mode. Fundamental expansions for computing the radial dependence in a slowly and uniformly rotating star were derived by Provost et al. (1981), Smeyers et al. (1981), and Saio (1982), all under the restriction $m \neq 0$.

The Sun has two “acoustic” cavities in which families of r modes would be trapped (Wolff & Blizard 1986). The outer cavity is most of the CE, and the inner cavity is most of the thick stable layers below the CE. With one exception, only modes in the inner cavity are discussed here. Wolff (2000) calculated a sample of 40 such modes to show how their radial and angular harmonic numbers (n, ℓ, m) affect cavity boundaries and amplitude distribution.

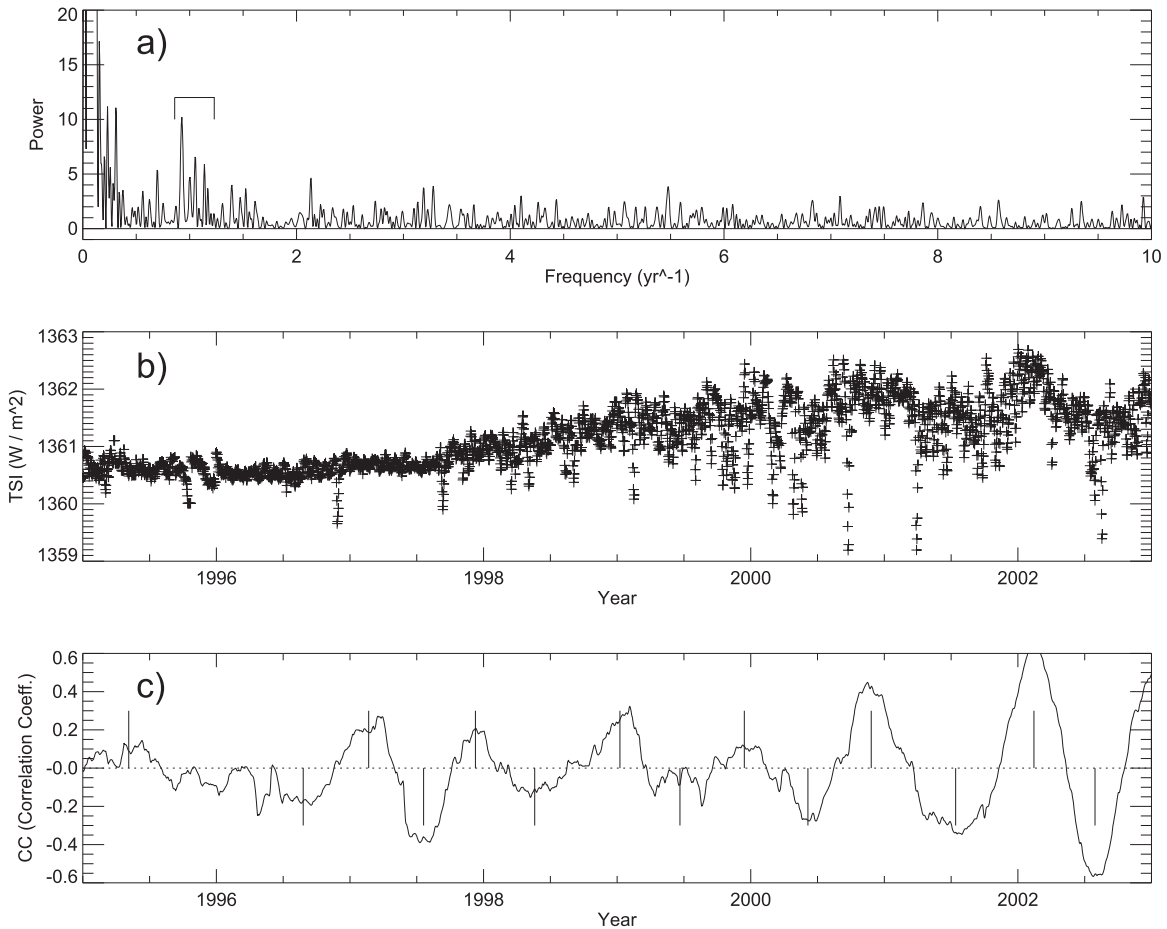


Figure 1. (a) The spectrum of the solar irradiance record (the PMOD composite series) has a cluster of power with periods near 1 yr. Most of the spectrum needs modification. (b) Daily values of irradiance for 8 yr. (c) The correlation coefficient (CC) between TSI and a 1 yr wavelet, F . The mean time of each annual peak or valley is defined by the vertical line that bisects its area. In one case near 1996.0, shorter-term fluctuations prevent marking a valley and peak.

The inner cavity rotates almost like a solid body as required in the classical r-mode derivations. Helioseismic analysis by Eff-Darwich & Korzenik (2013) determined the fluid rotation rate as $\nu_s = 431 \text{ nHz} = 13.60 \text{ yr}^{-1}$. Their observational uncertainty easily includes an independent measurement in Section 4.2 of $\nu_s = 13.59 \text{ yr}^{-1}$ based on a theoretical sequence of r-mode frequencies.

Saio (1982) gave the r-mode rotation frequency relative to inertial space,

$$\rho_\ell = \left[1 - \frac{2}{\ell(\ell+1)}\right]\nu_s. \quad (1)$$

This sidereal rate is also called the pattern speed and comes from the phase velocity of the mode's time-longitude dependence. Its rotation is perceived from Earth as the synodic frequency, $\rho_\ell - 1 \text{ yr}^{-1}$. The $\ell = 1$ mode is unique in that it does not rotate. Therefore, it appears from Earth as a retrograde rotation (period = -1 yr).

3. Analysis with Correlation Coefficient

The Fourier spectrum of solar irradiance (PMOD composite series) in Figure 1(a) has a conspicuous cluster of five closely spaced frequencies near 1 yr^{-1} , a possible sign of the r mode just mentioned. This region will be analyzed first in a very pedestrian manner to uncover details of the time variability including the waveforms of two modulations. Then, Section 4

will remove the stronger modulation and perform a standard spectral analysis.

3.1. The 1 yr Periodicity

An 8 yr sample of the composite TSI data is given in Figure 1(b), displaying typical behavior near a solar minimum and subsequent maximum. The TSI values were processed using a bandpass filter with about a 1 yr period, $F_k = \cos(2\pi\alpha\tau_k)$, where $\alpha = 1/364$ and τ_k runs from -182 to $+182$ in one-day steps. The array F_k was shifted, one day at a time, relative to TSI. At each step, j , a correlation coefficient was computed in terms of deviations from the mean of the 365 points involved at that step, namely, $\delta F_k \equiv F_k - \langle F \rangle$ and $\delta T_{j+k} \equiv TSI_{j+k} - \langle TSI \rangle_j$. The correlation coefficient at day j is

$$CC_j = \frac{\sum_k (\delta F_k \delta T_{j+k})}{(\sqrt{\sum_k (\delta F_k)^2})(\sqrt{\sum_k (\delta T_{j+k})^2})}. \quad (2)$$

Figure 1(c) shows the correlation coefficient (CC) for the same eight years. The mean time of each peak is defined by a vertical line that bisects the area between a positive section of the curve and the zero line (dotted). Similarly, negative sections define the time of each valley. In a few cases, one of these half-year pulses is distorted by an effect of a shorter timescale so that CC crosses the zero line and quickly returns. Such points were ignored if they persisted for ≤ 10 days (see Figure 1(c) at 1999.51); otherwise, the larger area was bisected (see 1996.45).

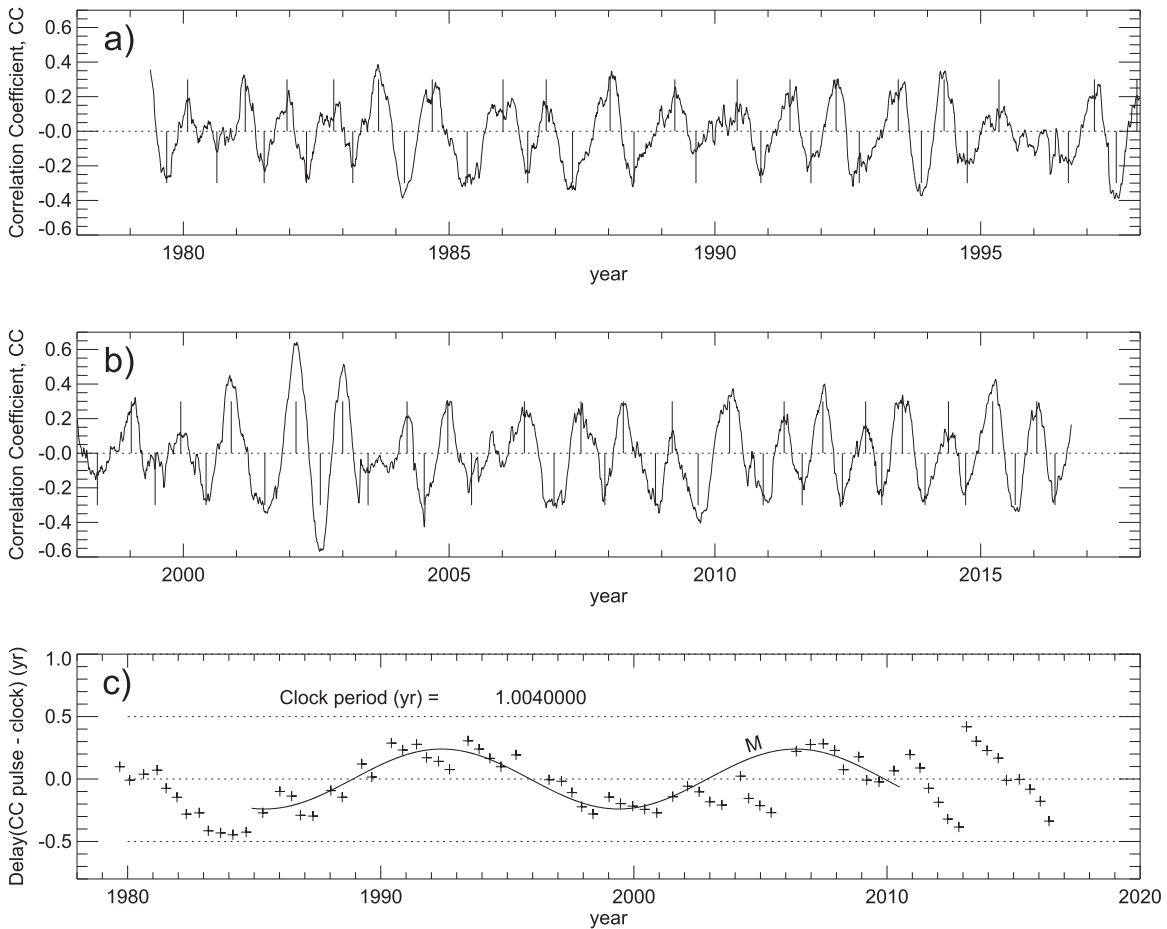


Figure 2. ((a) and (b)) A complete view of the correlation coefficient. Peaks and valleys recur at roughly 1 yr intervals. (c) The time delay of each peak or valley from the corresponding tick of a 1.004 yr clock. Delays follow a sinusoidal modulation, M, with a 14 yr period. A weaker modulation with a sawtooth waveform has a mean 2.6 yr recurrence. A new dominant periodicity of about 0.8 yr begins abruptly in 2010.

Area-based timing avoids depending only on the highest or lowest point of a feature, reducing the importance of large active regions suddenly rotating into or out of view of irradiance monitors. This limb effect does not represent a change in actual solar output.

Figures 2(a) and (b) show the entire CC curve. The roughly 1 yr recurrence of peaks is clear, but not surprising, as the filter mostly rejected frequencies outside the range, say, $1 \text{ yr}^{-1} \pm 30\%$. A more sensitive and revealing display in Figure 2(c) shows the delay of each CC event from the corresponding tick of a steady clock that ticks once every 1.004 yr. (The measured delay of each valley point has been increased by one half-period to align peaks and valleys into a more vertically compact string of points.)

From 1985 to 2010, the delay points mainly follow the modulating curve,

$$M(t) = (0.24 \text{ yr}) \cos 2\pi \frac{t - 2006.4}{14 \text{ yr}}, \quad (3)$$

with time t in years. In this analysis, 1.004 yr is not significantly different from 1.000 yr, but the latter clock produced points with a slight upward trend from 1985 to 2010. The 1.004 yr clock is deemed best at keeping pace with TSI because it leaves no secular trend.

The clock's phase, $t_0 = 2000.17$, is the time of any one of its ticks. Perturbing the phase merely moves all plotted points

vertically by the same amount. Phase was adjusted to approximately balance points above and below the curve M, ignoring several outlier points near 2005.

For at least 15 years a second modulation is visible with a sawtooth waveform and an amplitude about half that of M. We see it both as a modulation and later as a strong periodicity. Its recurrence time of about 2.6 yr matches that of the quasi-biennial oscillation (QBO). Qu & Xie (2013) identify it as a single line in their spectrum of solar radius data. Section 4 will confirm this. Others had viewed the QBO earlier as several changing frequencies, e.g., Obridko & Shelting (2001), when studying the solar wind sector structure.

3.2. The Full Extent of the 14 yr Modulation

The abrupt change on the delay plot after 2010 showed that TSI was no longer dominated by the 1.004 yr periodicity. A new value of about 0.8 yr became prominent. This is the approximate separation of the last seven peaks on the CC plot. For the best value, Figure 2(c) was replotted changing only the clock. Figure 3(a) shows the result for a clock period of 0.785 yr with phase $t_0 = 2000.40$. Post-2010 values closely follow M (extended as a dashed curve), so this clock value is adopted, but its accuracy is quite limited as it is observed for only seven years.

The pre-1985 delay points might represent a third periodicity. Its degree of agreement with a 0.956 yr clock with phase

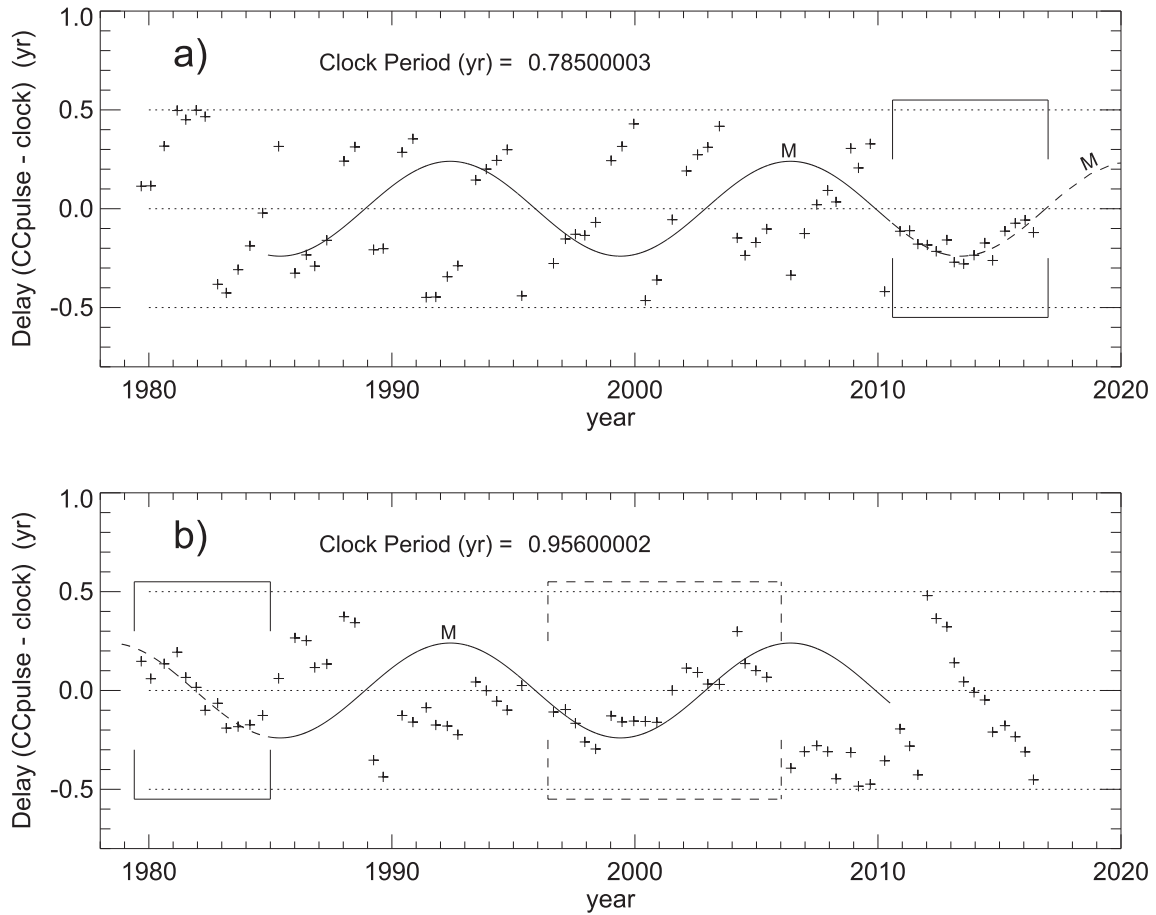


Figure 3. (a) From mid-2010 forward, the mean recurrence time is 0.785 yr. (b) Before 1985 there is some evidence for a 0.956 yr recurrence. This recurrence may also have a noticeable effect from 1996 to 2006, which means that it would exist simultaneously with the 1.004 yr effect. All three recurrences or periodicities mentioned so far align with the same 14 yr modulation curve, $M(t)$.

$t_0 = 2000.10$ can be seen within solid brackets in Figure 3(b). Its clock would tick at the same time as the 1.004 yr clock every 20.8 yr.

It appears that the modulator M affects the entire TSI record even as three different recurrence periods take turns having the strongest effect on TSI. Table 1 summarizes the delay plot results. Phase for clocks is the tick in the year 2000; for modulators, it is a time when they cause maximum delay.

Using the tabulated frequencies and phases of the 0.956 and 1.004 yr clocks, one finds that the two will tick simultaneously in 2001.22. Dashed brackets centered on this time are drawn in Figure 3(b), and the points inside roughly follow the curve M . So this interval has offered evidence for both clocks, one in Figure 3(b) the other in Figure 2(c). We will see below that the 0.956 effect is much weaker. The delay plot method detected it only when it was closer to being in phase with the stronger one than it was to being in antiphase.

4. Demodulated Lomb–Scargle (LS) Spectrum

4.1. Removing the Modulation

The modulation in Equation (3) has a peak to peak variation of $(2 \times 0.24/14) = 3.4\%$. So the two periodicities in Figure 3 that appear modulated by M will vary by about the same percentage if they remain active even when no longer dominant in TSI. To interpret this as frequency modulation (fm) of r-mode rotation rates, one could assume that layers below the

Table 1
Preliminary Results from CC Analysis

Frequency (yr^{-1})	Period (yr)	Phase (t_0)	Type
0.071	14.	2006.4	Modulator
0.38	2.6	1993.	Modulator
0.996	1.004	2000.17	Clock
1.046	0.956	2000.10	Clock
1.274	0.785	2000.40	Clock

CE change their rotation speed ν_s by 3.4% and therefore rotational energy by 6.9% during the 7 yr half-period of the modulation. Such huge, quick energy transfers $\sim 10^{34}$ J have no plausible source or sink.

More acceptable is delay modulation (dm), defined in the Appendix. Assume that 0.1% of the solar luminosity is temporarily held back inside the Sun for roughly half a decade because that is the observed change in TSI from solar maximum to solar minimum. For an extreme test, let all of this delayed energy be stored in a very thin layer immediately below the CE. Using a layer $0.01 R_\odot$ thick, where R_\odot is the solar radius, the fractional change in shell thermal energy will still only be $\sim 10^{-6}$. This presents no insuperable challenge.

As shown in the Appendix, a spectrum of the raw TSI record will be increasingly confusing at frequencies $\geq 1 \text{ yr}^{-1}$ due to

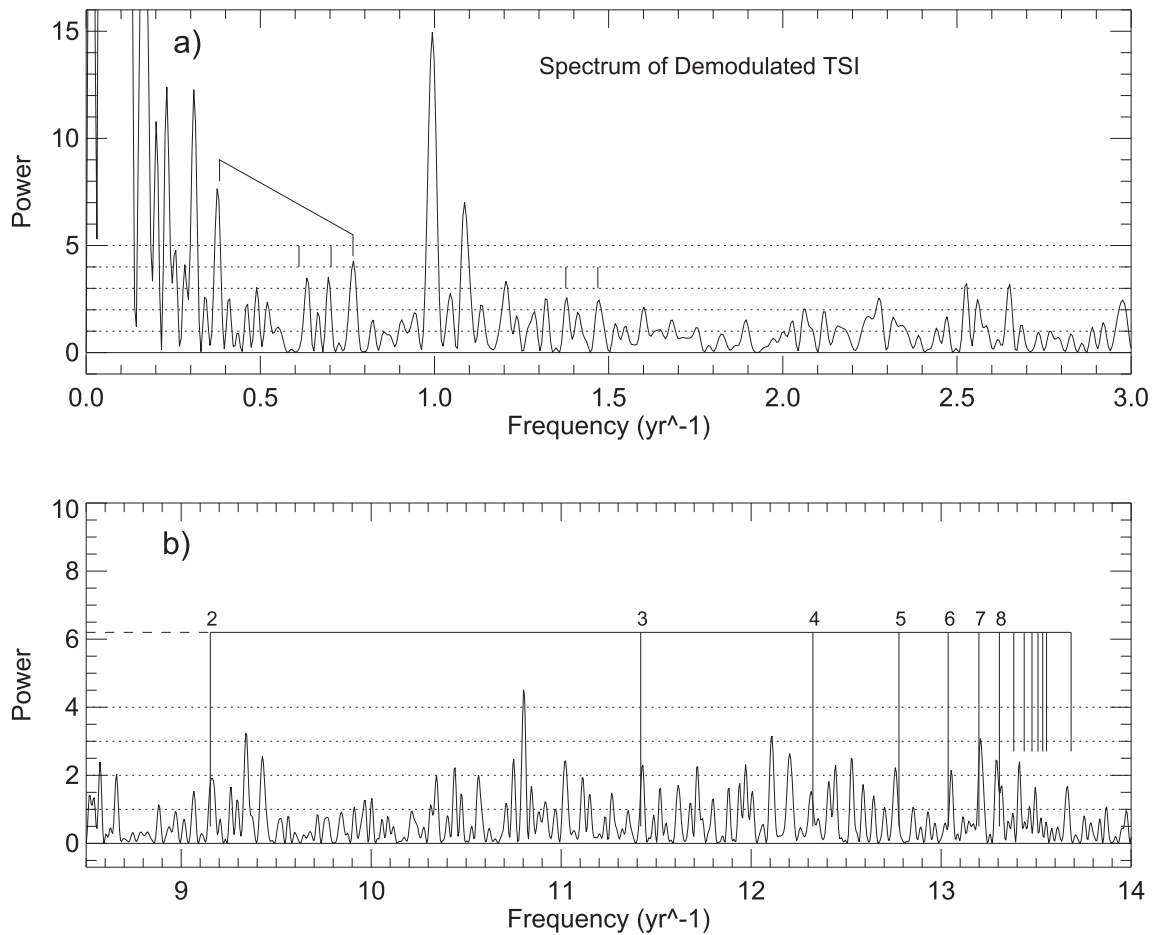


Figure 4. (a) The Lomb–Scargle spectrum of demodulated TSI reveals a powerful line at 0.994 yr^{-1} and a strong companion at 1.086 yr^{-1} . The weaker modulation (2.61 yr) remains. It is marked at 0.383 yr^{-1} , at its first harmonic, and at sideband locations for the two strong annual lines. (b) The sequence of beat frequencies between the deep r modes ($\ell = 2$ to 8) and the $\ell = 1$ r mode that can reach closest to the solar surface. They match lines in the LS spectrum.

sidebands from the 14 yr modulation. Sidebands can be greatly reduced by reversing the process used for Figure 5 and *subtracting* M from the time associated with each TSI value. This creates unequally spaced data points for which the LS method was designed. Figure 4 shows relevant parts of the LS spectrum of the demodulated TSI composite record. Two strong lines now dominate the annual range at frequencies, 0.994 and 1.086 yr^{-1} . Two of the three periodicities found by the delay method (Table 1) are detected again, this time without use of the filter F and CC . Table 2 gives some readings from the LS spectrum. It also confirms four of the six periodicities in the annual range reported by Lean & Brueckner (1989) from the extensive sunspot record.

Although this analysis removed perhaps 95% of the 14 yr modulation, the weaker sawtooth modulation still remains. It was not removed because its amplitude and phase are too ill-defined and it visibly affects only part of the TSI record. But its 2.61 yr period is conspicuous in the LS spectrum, accompanied by one harmonic (see the vertical marks at 0.383 yr^{-1} and twice that). Four more marks locate where the two tall annual-scale lines would have sidebands at $\pm 0.383 \text{ yr}^{-1}$. Three of them are visible.

4.2. Identification of r Modes

The TSI record measures only the absolute value of a frequency. It provides one value per day for the whole solar

Table 2
Some Annual-scale Periodicities in TSI

Frequency (yr^{-1})	Period (yr)	Power	Sunspots ^a (day)	Sunspots ^a (yr)
0.766	1.305	4.3
0.994	1.006	15.0
1.046	0.956	2.8	350	0.958
1.086	0.920	7.0	335.5	0.919
1.135	0.881	2.2	323.3	0.885
1.206	0.829	3.3
1.285	0.778	1.9	287	0.786

Note.

^a Lean & Brueckner (1989).

disk and does not tell whether a warm pattern on the Sun appears to drift eastward or westward. The strongest frequency, by far, in Table 2 is -0.994 yr^{-1} , which is almost exactly the expectation for an $\ell = 1$ r mode as pointed out in Section 2. Adding 1 gives the inertial rotation rate, $\rho_1 = +0.006 \text{ yr}^{-1}$, which is consistent with zero and Equation (1) as spectral readings have a formal uncertainty of $\pm 0.01 \text{ yr}^{-1}$ due to the 39 yr length of TSI data.

I consider this a detection of the $\ell = 1$ r mode below the CE, supported shortly by evidence for other r modes in that cavity. This is the most likely interpretation of such a powerful 1 yr

periodicity in solar irradiance. (Recall that TSI is already corrected for Earth's elliptical orbit.)

It is reasonable to assume that the other strong annual line at -1.086 yr^{-1} is the $\ell = 1$ mode, trapped in the CE and perturbed from -1.0 mainly by solar differential rotation. Its inertial rotation rate is $\rho_1^* = -0.086 \text{ yr}^{-1}$, where the asterisk identifies a CE mode.

The two modes of lowest degree rotate once around each other every $\approx 10.9 \text{ yr}$ according to the inverse of their beat frequency, $\rho_1 - \rho_1^*$. They interact in layers near the base of the CE where each mode extends an exponentially declining tail into the other acoustic cavity. Every 10.9 yr their velocity fields are parallel and reinforce each other. Then, 5.45 yr later they are antiparallel and suffer maximum cancellation. It follows that the ability of their combined flow field to interfere with convection in the interaction layers will vary on the same decadal scale. When spectral accuracy is improved, this beat may qualify as the long-term regulator of solar cycle lengths whose observed average value is 11.05 yr .

Many modes of higher ℓ might also be active in the inner cavity because it rotates almost like a rigid body. This keeps shear losses low and is required for full validity of the rotation law in Equation (1). Each mode will impose its motion near the base of the CE especially at mode antinodes. This gives special significance to the sequence of beat frequencies $\rho_\ell - \rho_\ell^*$ for $\ell = 1, 2, \dots$ because ρ_ℓ^* is the mode that gets closest to the surface, aiding detection. Figure 4(b) marks these theoretical beats for $\ell = 2$ to 14 for a fluid rotation rate, $\nu_s = 13.59 \text{ yr}^{-1}$, that agrees with helioseismology cited in Section 2. The series limit at $\ell = \infty$ is also marked.

The LS spectrum has lines matching the theory for $\ell = 1$ to 8 . (The $\ell = 1$ detection is far off scale at 0.092 yr^{-1} .) The observed sequence ends at its two tallest lines, $\ell = 7$ and 8 . This is consistent with the fact that modes of higher ℓ crowd closer to the boundary of the CE (Wolff 2000) where they can have more effect on convection and thus on solar irradiance. For $\ell \geq 9$ the modes might not be excited or the limited spectral resolution might prevent reliable detection.

5. Summary

Being aware that the lowest harmonic r mode stands still in inertial space when propagating in stellar layers rotating like a solid body, I thought that some solar observations taken near Earth might contain a -1.0 yr synodic periodicity. If so, a one-year clock would then be a stable test bed for measuring any active fm or delay modulation (dm). The modulation was interpreted as dm caused by a changing convective response time to local heat pulses deposited by global oscillations. A budding convective element finds it harder to get moving if there is a horizontal wind with a vertical gradient carrying some of its heat away. The r-mode velocities have this gradient near the edge of their acoustic cavity, which is near the base of the CE. This mechanism is complex and will require much detailed study.

After removing M from the TSI time axis to reduce confusing spectral sidebands, an LS spectrum (Figure 4(a), Table 2) showed that there are only two strong periodicities in the annual range: 1.006 and 0.920 yr . The two were identified as synodic rotation periods of the lowest-degree r mode ($\ell = 1$), each trapped in an acoustic cavity, respectively, below the CE and in the CE. Their rotation frequencies in inertial

space are $+0.006$ and -0.086 yr^{-1} with an uncertainty of about $\pm 0.01 \text{ yr}^{-1}$. The 0.006 yr^{-1} rate is consistent with zero, the ideal value for a rigidly rotating fluid. The other rate is perturbed from zero by the non-ideal conditions in the CE.

The 14 yr modulator appears to be active, independent of which periodicity is most prominent in affecting TSI (Figures 2(c) and 3). Its physical cause was not specified and it is too soon to know whether its 14 yr period is constant. A weaker sawtooth modulation with a 2.6 yr period could not be removed before forming the LS spectrum because it is too poorly defined by TSI data.

It will likely require many physical mechanisms to fully explain the irradiance variability. For example, vorticity from r modes can also change the efficiency of convection. Also, as their rotation rate, ρ , is independent of m, the m states of a given ℓ might couple, even if only very weakly, and rotate as a single more conspicuous entity analogous to a mechanism derived for asymptotic g modes by Wolff & ODonovan (2007). Several mechanisms will be explored in a more theoretical paper now in preparation.

I appreciate support of this publication by the Solar Physics Laboratory of Goddard Space Flight Center. I thank the referee for suggesting a better ordering of the manuscript. I am grateful to PMOD/WRC, Davos, Switzerland, for supplying their irradiance record (Frohlich 2006), composite_42_65_1709.dat, with new data from Virgo on the ESA/NASA Satellite Mission, *SOHO*.

Appendix Delay Modulation in the Sun

Electronic texts often discuss frequency modulation (fm) and phase modulation (pm), but I have not seen modulation of the time variable discussed. For example, thermal pulses applied periodically to the base of the Sun's CE would suffer a delay, perhaps variable, before their energy reaches the surface and contributes to solar irradiance. The 14 yr curve drawn in Figure 2(c) was modeled as delay modulation (dm) of periodic sources.

The modulation types, when sinusoidal, can be written in the same form: a wave $\sin(\omega t)$, perturbed by a modulating frequency Ω and a constant modulation index I to produce the signal,

$$S = \sin[\omega t + I \cos(\Omega t)], \quad (4)$$

where the omegas are constant and t is time. In phase modulation, I is defined as $\Delta\phi$, the maximum phase departure. In conventional fm, I is defined as $\Delta\omega/\Omega$, where $\Delta\omega$ is the maximum instantaneous deviation from the frequency ω . For fm this leads to well-known Bessel function solutions for the strength of each sideband vs frequency.

Analogous solutions should be possible for dm. Define its modulation index as

$$I = D\omega. \quad (5)$$

This leads to $S = \sin[\omega(t + D \cos \Omega t)]$, showing that D (a constant) is the maximum time-delay reached during this type of modulation.

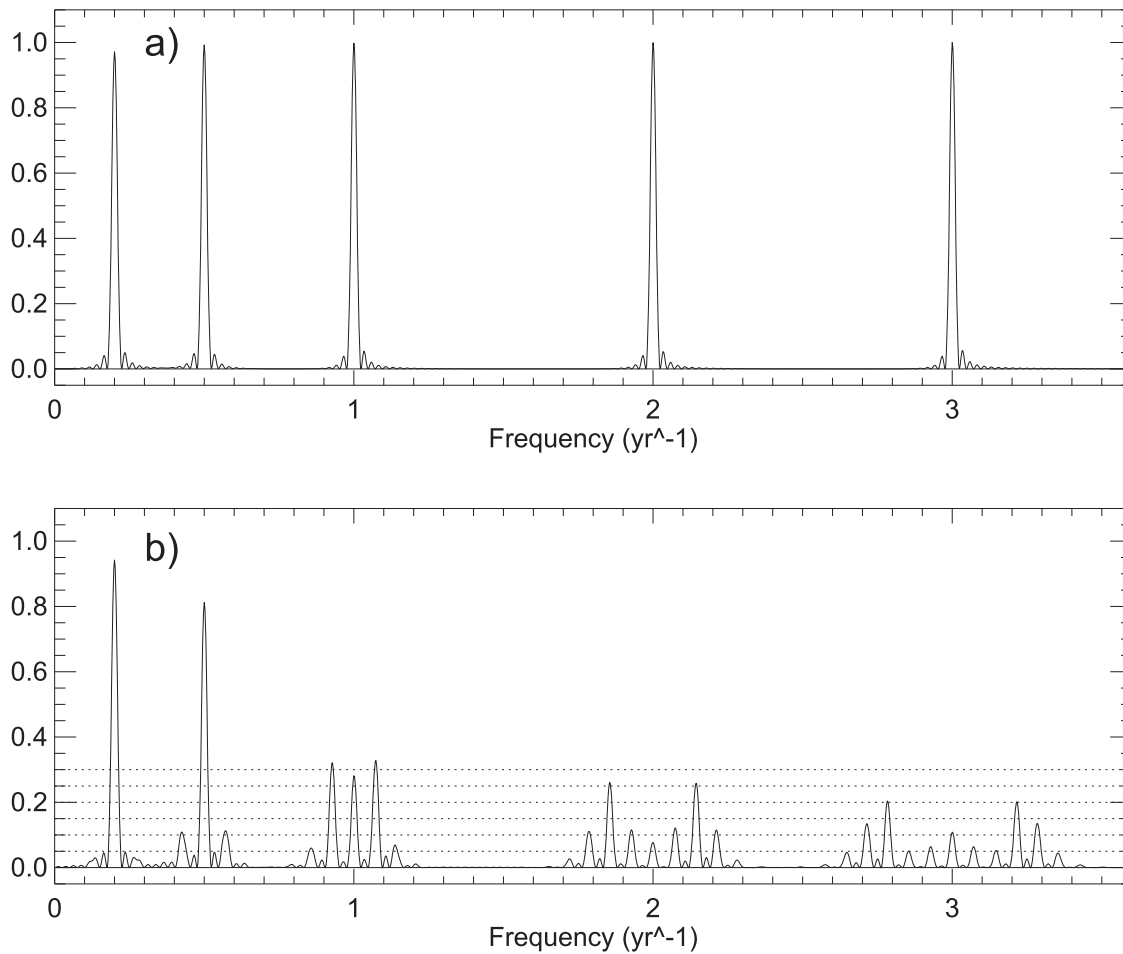


Figure 5. (a) The spectrum of five pure tones, sampled daily for 42 years. (b) The spectrum after the signal is modulated by the $M(t)$ found in solar irradiance. Sidebands are separated by 0.071 yr^{-1} , which is $(14 \text{ yr})^{-1}$. A simple FFT of the TSI record would be increasingly confusing for frequencies $\geq 1 \text{ yr}^{-1}$.

For solar irradiance, D is about 0.24 yr and $\Omega = 2\pi/14 \text{ yr}$ from the observed modulator M in Equation (3); see the main text. This applies to periodic thermal signals transmitted by convection across the entire CE and observed at the surface. It has a devastating effect on the detection of most spectral frequencies.

To see this, five waves, $\sin(\omega t)$, were summed to form a test signal and sampled daily for 42 years. Its fast Fourier transform (FFT) in Figure 5(a) shows the chosen frequencies, $\omega/2\pi$. The five waves were then distorted by the modulator into $\sin[\omega(t + M)]$. The test signal was sampled daily. Its FFT in Figure 5(b) shows the profusion of sidebands that erupt.

Sidebands are separated by $2\pi/14\text{yr}$ and their heights rise and fall as a function of ω , analogous to the Bessel solutions for fm. A spectrum of the raw TSI record will be increasingly confusing at frequencies $\geq 1 \text{ yr}^{-1}$.

ORCID iDs

Charles L. Wolff  <https://orcid.org/0000-0001-8854-507X>

References

- Bush, R. I., Emilio, M., & Kuhn, J. R. 2010, *ApJ*, **716**, 1381
 DeWitte, S., Crommelynck, D., Mekaoui, S., & Joukoff, A. 2004, *SoPh*, **224**, 209
 Eff-Darwich, A., & Korzennik, S. G. 2013, *SoPh*, **287**, 43
 Frohlich, C. 2006, *SSRv*, **125**, 53
 Frohlich, C., Crommelynck, D., Wehrli, C., et al. 1997, *SoPh*, **175**, 267
 Hickey, J. R., Stowe, L. L., Jacobowitz, H., et al. 1980, *Sci*, **208**, 281
 Kotov, V. A., & Levitsky, L. S. 1983, in *Solar and Magnetic Fields: Origins & Coronal Effects*, ed. J. Stenflo (Dordrecht: Reidel), 23
 Kuhn, J. R., Armstrong, J. D., Bush, R. I., & Scherrer, P. 2000, *Natur*, **405**, 544
 Lean, J. L., & Brueckner, G. E. 1989, *ApJ*, **337**, 568
 Obridko, V. N., & Shelting, B. D. 2001, *ARep*, **45**, 1012
 Oliver, R., Carbonell, M., & Ballester, J. L. 1992, *SoPh*, **137**, 141
 Provost, J., Berthomieu, G., & Rocca, A. 1981, *A&A*, **94**, 126
 Qu, Z. N., & Xie, J. L. 2013, *ApJ*, **762**, 23
 Saio, H. 1982, *ApJ*, **256**, 717
 Smeyers, P., Craeynest, D., & Martens, L. 1981, *Ap&SS*, **78**, 483
 Sturrock, P. A., Fischbach, E., Javorek, D., II, et al. 2014, *Aph*, **59**, 47
 Willson, R. C., & Hudson, H. S. 1988, *Natur*, **332**, 810
 Willson, R. C., & Mordvinov, A. V. 2003, *GeoRL*, **30**, 1199
 Wolff, C. L. 2000, *ApJ*, **531**, 591
 Wolff, C. L., & Blizard, J. B. 1986, *SoPh*, **105**, 1
 Wolff, C. L., & ODonovan, A. E. 2007, *ApJ*, **661**, 568